Magn Reson Med Sci
doi:10.2463/mrms.tn.2022-0063
Published Online: November 17, 2022

TECHNICAL NOTE

Ultra-short Echo-time MR Angiography Combined with a Modified Signal Targeting Alternating Radio Frequency with Asymmetric Inversion Slabs Technique to Assess Visceral Artery Aneurysm after Coil Embolization

Kohei Hamamoto[1,2*], Emiko Chiba[3], Noriko Oyama-Manabe[2], Hironao Yuzawa[2], Hiromi Edo[1], Yohsuke Suyama[1], and Hiroshi Shinmoto[1]

Contrast-enhanced CT and MR angiography are widely used for follow-up of visceral artery aneurysms after coil embolization. However, potential adverse reactions to contrast agents and image deterioration due to susceptibility artifacts from the coils are major drawbacks of these modalities. Herein, we introduced a novel non-contrast-enhanced MR angiography technique using ultra-short TE combined with a modified signal targeting alternating radio frequency with asymmetric inversion slabs, which could provide a serial hemodynamic vascular image with fewer susceptibility artifacts for follow-up after coil embolization.

Keywords: *coil embolization, non-contrast-enhanced magnetic resonance angiography, ultra-short echo-time*

Introduction

Transcatheter coil embolization has become the first-line therapy for visceral artery aneurysms (VAAs) because it is less invasive than surgical treatment. However, the risk of recanalization of blood flow at embolized lesions of up to 26% due to coil compaction or thrombolysis is a major concern in coil embolization.[1–5] Therefore, the periodic assessment of the residual blood flow in treated lesions is required.

Various modalities have been used as follow-up evaluation methods after coil embolization of VAAs, including CT, MR angiography (MRA), ultrasonography (US), and digital subtraction angiography (DSA).[1,2,6–8] Traditionally, DSA has been used as an evaluation method after endovascular treatment. However, DSA is not routinely performed because of its invasiveness. Contrast-enhanced CT and MRA are widely used in follow-up studies of treated VAAs due to their low invasiveness and high spatial resolution.[2,6,8,9] More recently, the utility of time-resolved contrast-enhanced MRA (TR-CEMRA) has also been reported, which can provide hemodynamic information, for follow-up assessment after embolization.[10] However, some limitations are associated with the use of iodine- or gadolinium-based contrast media, such as the increased risk of adverse reactions in patients with a history of allergies or renal insufficiency.

A non-contrast-enhanced MRA technique using 3D-balanced steady-state free precession MRA with arterial spin labeling (ASL) has recently been applied to evaluate renal artery aneurysms after coil embolization.[11] More recently, the utility of ultra-short echo-time (UTE) MRA has been reported, which is less susceptible to magnetic susceptibility artifacts due to metallic materials, to evaluate a renal artery aneurysm treated with metallic coils.[12] However, a major limitation of these techniques is that they only perform a single scan without serial hemodynamic imaging. Moreover, the feasibility of using non-contrast-enhanced MRA to evaluate treated VAAs other than the renal artery has not been elucidated.

Herein, we introduced a novel non-contrast-enhanced MRA technique using UTE MRA combined with modified signal targeting alternating radio frequency with asymmetric inversion slabs (UTE-mASTAR MRA), which enabled the reduction of susceptibility artifacts and the acquisition of serial hemodynamic images for evaluating various VAAs treated with metallic coils.

[1]Department of Radiology, National Defense Medical College, Tokorozawa, Saitama, Japan
[2]Department of Radiology, Jichi Medical University Saitama Medical Center, Saitama, Saitama, Japan
[3]Department of Radiology, National Center Hospital, National Center of Neurology and Psychiatry, Kodaira, Tokyo, Japan
*Corresponding author: Department of Radiology, National Defense Medical College, 3-2, Namiki, Tokorozawa, Saitama 359-8513, Japan. Phone: +81-4-2995-1689, Fax: +81-4-2996-5214, E-mail: hkouhei917@gmail.com

Received: May 16, 2022 | Accepted: September 25, 2022

Table 1 Summary of patient profiles, lesions, embolization technique.

Case	Age, gender	Lesion type	Location	Aneurysm size (H × L × W) (mm)	Embolization technique
1	63, M	RAA	Left upper	27 × 16 × 24	CP with PP
2	49, M	SAA	Distal	24 × 19 × 17	CP with PP
3	66, M	SAA	Middle	32 × 25 × 22	CP with PP
4	71, F	SAA	Middle	33 × 26 × 17	Isolation and rough CP
5	71, F	PHAA	Middle	22 × 17 × 12	Isolation and rough CP

CP, coil packing; F, female; H, height; L, length; M, male; PHAA, proper hepatic artery aneurysm; PP, preserving the parent artery circulation; RAA, renal artery aneurysm; SAA, splenic artery aneurysm; W, width.

Materials and Methods

This retrospective case series was approved by our institutional review board and adhered to the principles of the Declaration of Helsinki. The need for informed consent was waived due to the retrospective study design.

Patient and aneurysm characteristics

Between October 2019 and March 2021, five VAAs treated with metallic coils, which underwent UTE-mASTAR MRA and TR-CEMRA for post-treatment evaluation, were included. Patient characteristics and embolization techniques are summarized in Table 1. VAAs were diagnosed in all patients using contrast-enhanced CT. Indications for treating VAAs were determined based on a previous study[13] and included aneurysm with a diameter of 2 cm or more, symptoms attributable to aneurysms, an increasing aneurysm size, and childbearing age. The VAAs were localized within the renal artery (n = 1), splenic artery (n = 3), and proper hepatic artery (n = 1). All VAAs were saccular and embolized with 0.010–0.020-inch platinum coils. Selective embolization of the aneurysm with preservation of the parent arteries was performed in three VAAs. In two VAAs, an isolation technique that occluded the parent artery both distally and proximally to the aneurysm embolization was performed. In all VAAs, complete embolization of the aneurysmal body and absence of organ infarction were confirmed by DSA at the end of the embolization procedure. We evaluated all patients based on UTE-mASTAR MRA and TR-CEMRA, performed approximately two to three months postoperatively (mean 78.6 days, range 61–85 days). No patients underwent DSA after embolization because no evidence of recanalization of the aneurysmal body was observed on both UTE-mASTAR MRA and TR-CEMRA.

MRA scan technique

All MRAs were performed on a 3T MRI scanner (Vantage Titan 3T; Canon Medical Systems, Tochigi, Japan) using a 16-channel phased-array coil (Atlas SPEEDER Body; Canon Medical Systems) combined with a 40-channel phased-array coil (Atlas SPEEDER Spine). UTE-mASTAR and TR-CEMRA were performed consecutively during the same examination. To determine the acquisition area and the location for placement of ASL pulse, axial, coronal, and sagittal field echo images without an inversion pulse were acquired using the following parameters: TR/TE, 50/2.3; flip angle, 30°; FOV, 400 × 400 mm; matrix, 256 × 128; number of slices, 7; and slice thickness, 10 mm.

UTE-mASTAR MRA

For UTE MRA, we conducted a 3D-minimized acoustic noise utilizing UTE (mUTE), one of the UTE sequences, because mUTE could provide higher temporal resolution images without image deterioration than those provided by conventional UTE (unpublished data based on our institutional experience). In mUTE, the center of the k-space is filled with Cartesian acquisition, and the periphery is filled with radial acquisition, whereas all k-spaces are filled with radial acquisition in conventional UTE. The scan parameters of the mUTE are listed in Table 2. mASTAR is an ASL technique that was used as a preparation pulse and provided multi-phase MRA images during one session.[14] For UTE-mASTAR MRA imaging, 3D UTE images with and without ASL (tag) pulse were acquired alternately in the same slice plane, generating separate images. The images with tag pulses were acquired with multi-step delay times which were then individually reconstructed and subtracted to yield the final angiogram; this allows depiction of only blood signals from the tagged region by cancellation of the background signal via subtraction. Consequently, this technique can provide serial hemodynamic MRA images, which are referred to as UTE-mASTAR MRA images. Figure 1 shows the image acquisition and reconstruction procedure. For image acquisition, respiratory bellows gating was applied at the beginning of expiration. Due to a limitation in the acquisition volume of UTE-mASTAR MRA during one session, we set the position of each slab to include the targeted VAAs and the proximal and distal portions of the parent artery by referring to the pre-treatment images (contrast-enhanced CT or MRI). The tag pulse was placed in the range that covered the abdominal aorta and proximal portion of the targeted VAAs. The position and thickness of the tag

Table 2 MR angiography scan parameters.

	UTE-mASTAR MRA	TR-CEMRA
TR/TE (ms)	3.0/0.100	3.7/1.3
Flip angle (°)	5	20
Section thickness (mm)	1[a]	1.25[b]
FOV (mm)	350 × 350	370 × 370
Matrix size	256 × 256[c]	512 × 320[c]
Parallel imaging factor	1	2
Acquisition voxel size (mm)	0.68 × 0.68 × 1	0.72 × 1.16 × 1.25
Number of slices	80 (to cover the embolized lesions)	40 (to cover the embolized lesions)
Signal acquired (n)	2	1
Number of coverages	1	1
Number of segments	100	1000
Number of trajectories	9600	N/A
Imaging plane	Axial	Coronal
Imaging time	12–13 min	24s

[a]The acquired slice sections of 2 mm were reconstructed with 1.0 mm voxel intervals by mid-slice reconstruction. [b]The acquired slice sections of 2.5 mm were reconstructed with 1.25 mm voxel intervals by mid-slice reconstruction. [c]Reconstruction matrix. N/A, not applicable; TR-CEMRA, time-resolved contrast-enhanced MR angiography; UTE-mASTAR MRA, ultra-short TE MR angiography combined with modified signal targeting with alternative radio frequency with asymmetric inversion slabs technique.

pulse depended on the morphology of the abdominal aorta and the position of the VAAs. After the tag pulse application, the delay times were set at 200, 506, and 812 ms. In UTE-mASTAR MRA, the delay time interval and the number of time phases depend on the number of segments. However, there is a trade-off between the number of segments and imaging time. Therefore, we determined the optimal number of delay time intervals and time phases that would allow appropriate hemodynamic evaluation with reasonable imaging time using volunteers prior to the current study.

TR-CEMRA

TR-CEMRA was performed using a 3D fast field-echo sequence in conjunction with a parallel imaging technique and segmented k-space sampling technique.[15] The scan parameters for this sequence are listed in Table 2. Due to the limitation in the acquisition volume of TR-CEMRA, we set the position of each slab to include the target VAAs by referring to recent contrast-enhanced CT images, as in UTE-mASTAR MRA. The temporal resolution for each 3D dataset in TR-CEMRA was 3s, and eight dynamic scans were obtained during 24s of breath-holding at end inspiration. Data acquisition began 10s after an injection of 0.1 mmol/kg of gadobutrol (Gadovist; Bayer HealthCare, Whippany, NJ, USA) or gadoteridol (ProHance; Esai, Tokyo, Japan) at a flow rate of 2 mL/s via a right median cubital vein, followed by a saline flush of 40 mL during breath-holding.

DSA

All DSAs were performed with an image flat-panel fluoroscopy system (Infinix Celeve-i INFX-8000; Canon Medical Systems) using iodinated contrast agent (Oypalomin 300 or 350; Fuji Pharma, Tokyo, Japan). Evaluation of the VAAs before and after coil embolization was performed by 2D DSA from multiple view angles using a 4-French catheter. The fame rate was set at 5 frames/s.

Phantom study

To determine and compare the capability of UTE-mASTAR MRA and TR-CEMRA in detecting intra-aneurysmal blood flow signals after coil embolization, we performed a phantom study using an aneurysm model. The acrylic aneurysm model was created based on a 3D image of actual visceral aneurysms (FUYO, Tokyo, Japan). The aneurysm diameter was 12 × 10 × 10 mm, the neck diameter was 5 mm, and that of the parent artery was 5 mm. The 0.014-inch platinum coils (Target XL 360; Stryker, Cork, Ireland) were placed in the aneurysm phantom with a volume embolization ratio of approximately 12%. The scan parameters were the same as those used in the patient study. For imaging of UTE-mASTAR MRA, the phantom model was imaged under pulsatile conditions with a diluted gadolinium-diethylenetriamine pentaacetic acid (Gd-DTPA) solution that simulated the T1 value of blood (T1 value = 1600 ms).[16] For TR-CEMRA imaging, the fluid in the phantom was changed to a diluted Gd-DTPA solution that simulated a

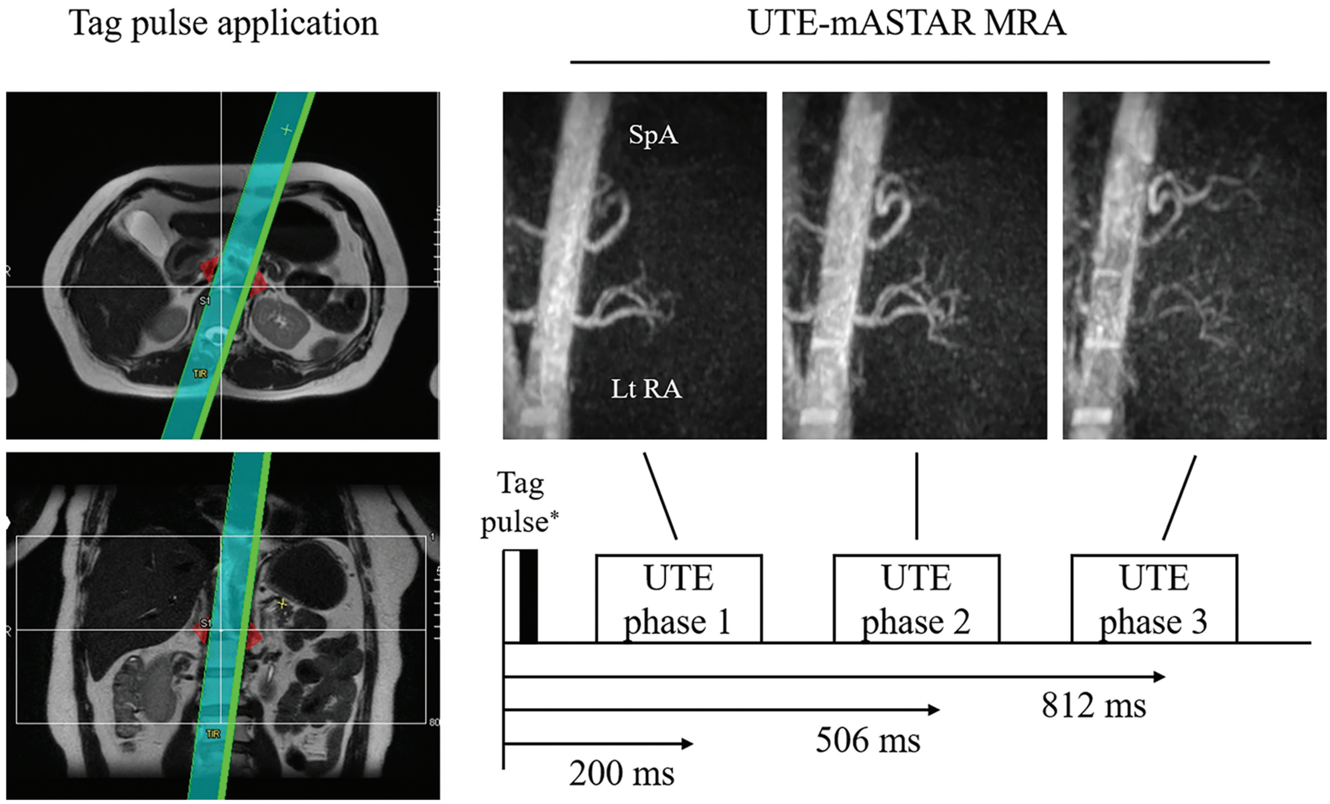

Fig. 1 Procedure for acquiring UTE-mASTAR MRA. 3D UTE images acquired with and without tag pulse (asterisk) were acquired alternately for each segment of the same slice at 200, 506, and 812 ms of delay time after applying the tag pulse (green parallelogram). The tag pulse was placed on the range that covered the abdominal aorta and proximal portion of the target arteries. These images were subtracted; consequently, only signals of the targeted arteries were described on UTE-mASTAR MRA images. Note that the peripheral portions of the SpA and the Lt RA are gradually visualized from phase 1 to phase 3 on UTE-mASTAR MRA. Lt RA, left renal artery; SpA, splenic artery; UTE-mASTAR MRA, ultra-short TE MR angiography combined with modified signal targeting alternating radio frequency with asymmetric inversion slabs.

contrasted blood vessel (T1 value = 300 ms).[17] The average flow rate was 2.8 mL/s, simulating visceral arteries.[18] For creating a pulsatile Gd-DTPA solution flow, we used a pulsating flow pump (ALPHA FLOW EC-2; FUYO) and pulsating flow controller (ALPHA FYC EC-2; FUYO). The pulse frequency was set at 60 cycles/min. DSA images with iodine contrast agent (Oypalomin 300; Fuji Pharma) under the same flow conditions were used as standard reference images. The parameters of DSA were set as in the clinical cases.

Image assessment

All MRA data were transferred to a picture archiving and communication system viewer (Synapse EX-V, Fujifilm Medical, Tokyo, Japan) equipped with multiplanar reconstruction (MPR) and maximum intensity projection (MIP) for source images. The images were independently analyzed by two experienced interventional radiologists with ten and eight years of experience as readers one and two, respectively. Image analyses were performed by using partial MIP images focused on the target regions and MPR images in order to minimize the effect of overlap of organs and background signals. For the patient study, MRA image analysis was conducted side-by-side comparing the partial MIP and MPR image of each MRA with the DSA image after coil embolization and preoperative contrast CT. First, the image quality of UTE-mASTAR MRA and TR-CEMRA for the visualization of target arteries (parent arteries of the VAAs and proximal arteries contiguous with the parent arteries) was scored on a four-point scale (1 = non-diagnostic, no visualization of target vessels; 2 = fair, detectable of target vessels but not clear; 3 = good, confident identification of target vessels; and 4 = excellent, sharp visualization of target vessels). Images with scores of three and four were considered appropriate for evaluation after coil embolization. Second, the intra-aneurysmal flow was graded on a three-point scale according to Roy's classification: residual aneurysm (inflow signal detected in the aneurysmal dome), residual neck (inflow signal detected in the aneurysmal neck), and complete occlusion (no inflow signal detected in the aneurysm).[19] Third, the hemodynamic status, such as the collateral, distal, and parent arterial circulation status, was evaluated using a three-point scale: occluded (parent artery

Table 3 Embolization follow-up outcome on UTE-mASTAR MRA and TR-CEMRA.

Case	Image quality score				Embolization follow-up outcome				Comparison of visibility of blood flow signals	
	UTE-mASTAR MRA		TR-CEMRA		UTE-mASTAR MRA		TR-CEMRA			
	Reader 1	Reader 2	Reader 1	Reader 2	Reader 1	Reader 2	Reader 1	Reader 2	Reader 1	Reader 2
1	4	4	4	4	RN with CPPA	RN with CPPA	RN with CPPA	RN with CPPA	1	1
2	4	4	4	4	CO with CPPA	CO with CPPA	CO with PPPA	CO with PPPA	1	1
3	4	4	4	4	RN with CPPA	RN with CPPA	RN with CPPA	RN with CPPA	2	2
4	4	4	4	4	CO with CPDA	CO with CPDA	CO with PPDA	CO with PPDA	1	1
5	4	4	3	3	CO with CPDA	CO with CPDA	CO with ODA	CO with ODA	1	1

CO, complete occlusion; CPDA, confidentially patent of distal artery; CPPA, confidentially patent of parent artery; ODA, occlusion of distal artery; PPDA, probably patent of distal artery; PPPA, probably patent of parent artery; RN, residual neck; TR-CEMRA, time-resolved contrast-enhanced MR angiography; UTE-mASTAR MRA, ultra-short TE MR angiography combined with modified signal targeting with alternative radio frequency with asymmetric inversion slabs technique.

or distal artery are not visualized), probably patent (hemodynamic imaging shows the proximal and distal parts of the parent artery almost simultaneously, but the continuity is unclear, or collateral and distal artery are visualized but the continuity is unclear), and confidentially patent (the continuity of the parent artery or the continuity of the collateral and distal arteries is clearly visualized). Finally, the capability of UTE-mASTAR MRA and TR-CEMRA to depict blood flow signals in the aneurysm or parent arteries adjacent to the coils was compared using a three-point categorical scale (1, UTE-mASTAR MRA is superior to TR-CEMRA; 2, UTE-mASTAR MRA is almost equivalent to TR-CEMRA; and 3, UTE-mASTAR MRA is inferior to TR-CEMRA). For the phantom study, the intra-aneurysmal flow signals observed by UTE-mASTAR MRA and TR-CEMRA were assessed using a five-point scale by comparing with DSA images: 1, not visible (signal alteration in the aneurysm was not detected or could not be assessed); 2, poor (blood flow signals in the aneurysm were slightly visible, but not adequate for diagnosis); 3, acceptable (blood flow signals in the aneurysm were partially visible, diagnosable images); 4, good (blood flow signals in the aneurysm were roughly visible, but limited compared with DSA); and 5, excellent (the images were almost equal to DSA). Subsequently, the detectability of UTE-mASTAR MRA and TR-CEMRA for intra-aneurysmal blood flow signals was compared using a three-point categorical scale as in the patient study (1, UTE-mASTAR MRA was superior to TR-CEMRA; 2, UTE-mASTAR MRA was almost equivalent to TR-CEMRA; and 3, UTE-mASTAR MRA was inferior to TR-CEMRA), with reference to DSA. Comparisons between DSA and MRA were performed by using the 2D-DSA images obtained from four directions (0°, 45°, 90°, and 135°) and partial MIP images of MRAs reconstructed at the corresponding angles. In addition, we calculated and compared the volume of blood signal in the aneurysm phantom for each MRA using a workstation (VINCENT; Fujifilm Medical). The blood flow signals within the aneurysm phantom of MRAs were manually extracted to distinguish them from the background signal and the parent artery using MIP images set to the appropriate window level and width, and volumetric analysis was performed. Subsequently, these values were compared to the estimated residual blood flow volume of the aneurysm phantom calculated by the following formula: (total blood volume of the aneurysm phantom before coil placement calculated from the original data) × (1 – volume embolization ratio/100).

Results

All patients underwent UTE-mASTAR MRA without any difficulty. The image quality score ratings and embolization follow-up outcomes are summarized in Table 3. The median image quality score of UTE-mASTAR MRA was four (interquartile range, 4–4; range, 4–4), which was almost equal to that of TR-CEMRA, four (interquartile range, 4–4; range, 3–4). UTE-mASTAR MRA provided serial hemodynamic vascular images of target vessels in all cases. For the evaluation of aneurysm occlusion, UTE-mASTAR MRA showed complete occlusion in three cases and residual neck in two cases, which were in good agreement with the findings of TR-CEMRA. To evaluate the hemodynamic status following embolization, UTE-mASTAR MRA determined

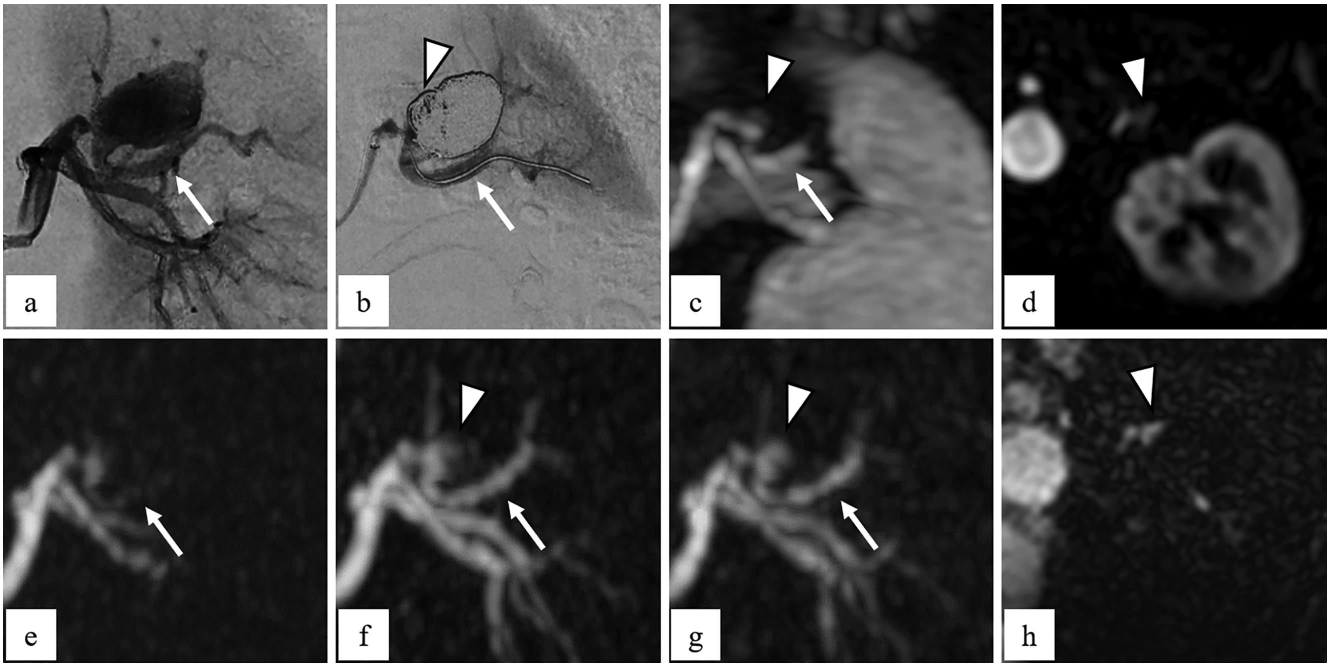

Fig. 2 A 63-year-old man with a left renal artery aneurysm (Case 1). (**a**) DSA of the left renal artery shows a saccular aneurysm in the upper branch. The arrow indicates the distal portion of the parent artery. (**b**) DSA after coil embolization using a neck preservation technique attains almost complete embolization of the aneurysm, except for a small neck remnant (arrowhead) and patency of the parent artery (arrow). (**c** and **d**) Follow-up TR-CEMRA was performed three months after initial embolization (**c**, partial MIP image on coronal view; **d**, MRP image on axial view). A small contrast effect was detected within the aneurysm neck (arrowheads in **b** and **c**), suggesting the residual neck. The parent artery is preserved (arrow in **c**). (**e**–**h**) UTE-mASTAR MRA (**e**–**g**, MIP image on coronal view; **h**, MPR image on axial view). The delay time of images (**e**), (**f**), (**g**), and (**h**) was 200, 506, 812, and 812 ms, respectively. The continuity of the parent artery is clearly visualized, and the distal portion of the parent artery is gradually visualized as well as other renal artery branches (arrows in **e**–**g**). Residual blood flow signals are seen at the aneurysmal neck, indicating the residual neck (arrowheads in **f** and **g**). Note that UTE-mASTAR MRA depicts the residual blood flow signal more clearly than that depicted by TR-CEMRA (arrowheads in **c**, **d**, **g**, and **h**). DSA, digital subtraction angiography; MIP, maximum intensity projection; MRP, multiplanar reconstruction; TR-CEMRA, time-resolved contrast-enhanced MRA; UTE-mASTAR MRA, ultra-short TE MR angiography combined with modified signal targeting alternating radio frequency with asymmetric inversion slabs.

that the parent arteries remained patent in all patients who underwent coil packing of the aneurysm with a preserved parent artery (n = 3) (Figs. 2 and 3). Conversely, TR-CEMRA determined that the parent artery was patent based on the findings of hemodynamic images in all cases with coil packing, but the continuity of the parent artery adjacent to the coils was unclear in one case of the splenic artery (Fig. 3). In patients who underwent parent artery occlusion (isolation technique), both UTE-mASTAR MRA and TR-CEMRA revealed complete emboli in all cases (n = 2). Regarding the visibility of the distal arteries, UTE-mASTAR MRA could visualize the distal arteries in all cases (Fig. 4), whereas TR-CEMRA could not visualize the distal arteries in a case with a proper hepatic artery aneurysm (Fig. 5). Comparing the visibility of blood flow signals adjacent to the coils, both readers rated a score of one in four cases (Figs. 2–5) and two in one case.

In the aneurysm phantom study, both readers rated a score of four on both UTE-mASTAR MRA and TR-CEMRA images (Fig. 6). When comparing the visibility of intra-aneurysmal blood flow signals, both readers rated a score of one. The calculated blood flow signal volume of UTE-mASTAR MRA in the aneurysm phantom was 570 mm^3, which was higher than that of TR-CEMRA (340 mm^3). In addition, the value of UTE-mASTAR MRA was similar to the estimated residual blood flow volume (574 mm^3).

Discussion

In this report, UTE-mASTAR MRA using the ASL technique provided hemodynamic information and enabled clear visualization of intra-aneurysm residual blood flow and the parent artery after coil embolization. Moreover, this technique provides fewer susceptibility artifacts from metallic coils than TR-CEMRA. These findings indicate that the UTE-mASTAR MRA is useful for assessing VAAs after treatment with metallic coils.

UTE MRA is a relatively new MRA method that is reportedly useful for minimizing susceptibility artifacts due to ultra-short TE (TE < 0.1 ms). This sequence can reduce the phase dispersion due to metallic substances, providing fewer susceptibility images even after endovascular treatment

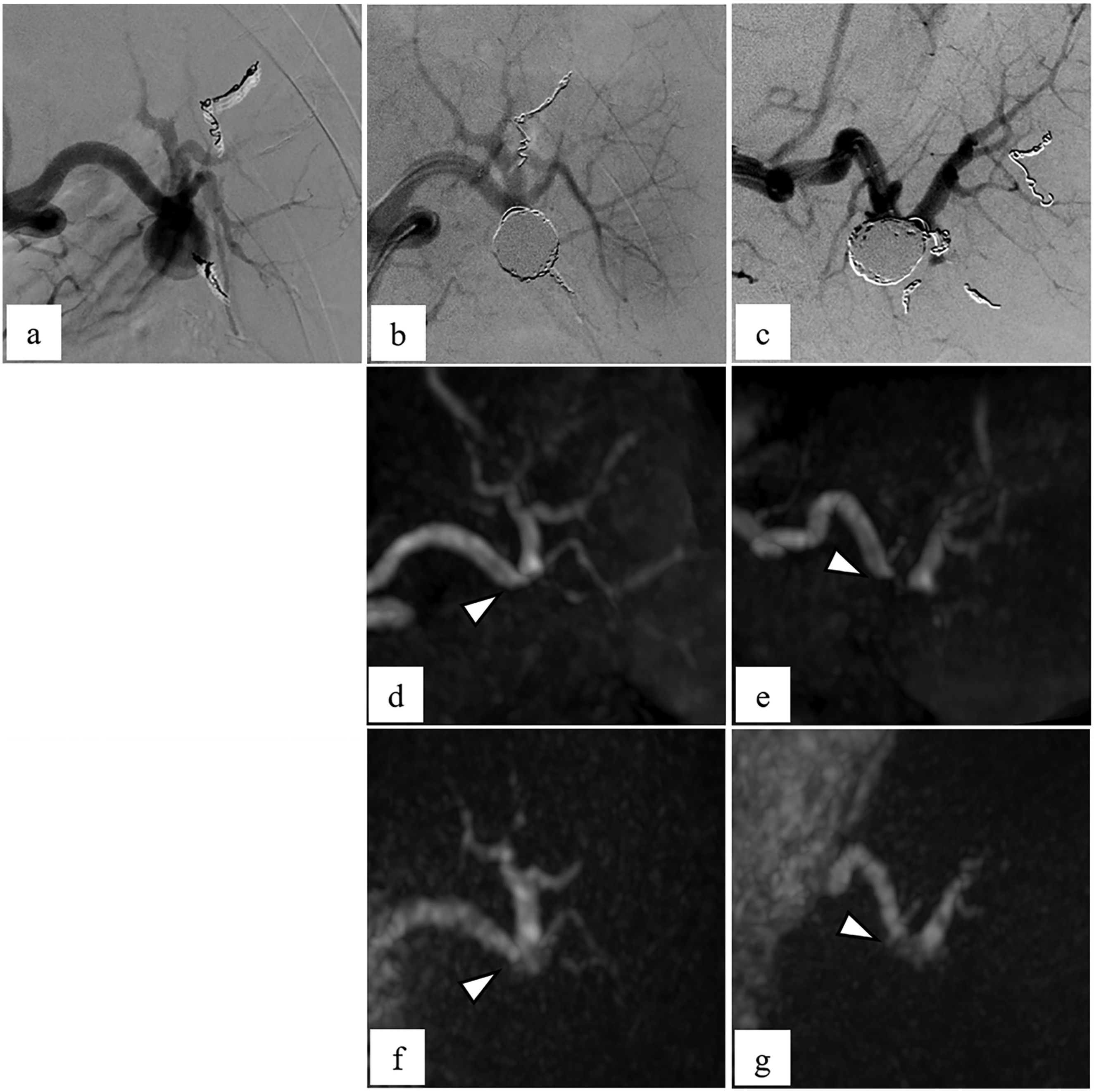

Fig. 3 A 49-year-old man with a splenic artery aneurysm (Case 2). (**a**) Pre-treatment DSA of celiac artery of the left cranial view. (**b** and **c**) DSA of the left cranial view (**b**) and right cranial view (**c**) after coil embolization using a neck preservation technique showing complete embolization of the aneurysm and patency of the parent artery. (**d** and **e**) Follow-up TR-CEMRA performed three months after coil embolization (partial MIP image). The view angles are corresponding to DSA (**d**, left cranial view; **e**, right cranial view). No contrast effect is detected in the aneurysm, indicating complete occlusion. The proximal and distal portions of the parent arteries of the aneurysm are simultaneously visualized, suggesting the patent parent artery. However, the continuity of the parent artery is unclear in the part adjacent to the coils (arrowheads). (**f** and **g**) UTE-mASTAR MRA with a delay time of 812 ms (partial MIP image). The view angles are corresponding to DSA and TR-CEMRA (**f**, left cranial view; **g**, right cranial view). No evidence of aneurysmal recanalization as well as TR-CEMRA. The continuity of the parent artery adjacent to the coil is clearly visualized, which allows for a reliable diagnosis of the patency of the parent artery (arrowheads). DSA, digital subtraction angiography; MIP, maximum intensity projection; TR-CEMRA, time-resolved contrast-enhanced MRA; UTE-mASTAR MRA, ultra-short TE MR angiography combined with modified signal targeting alternating radio frequency with asymmetric inversion slabs.

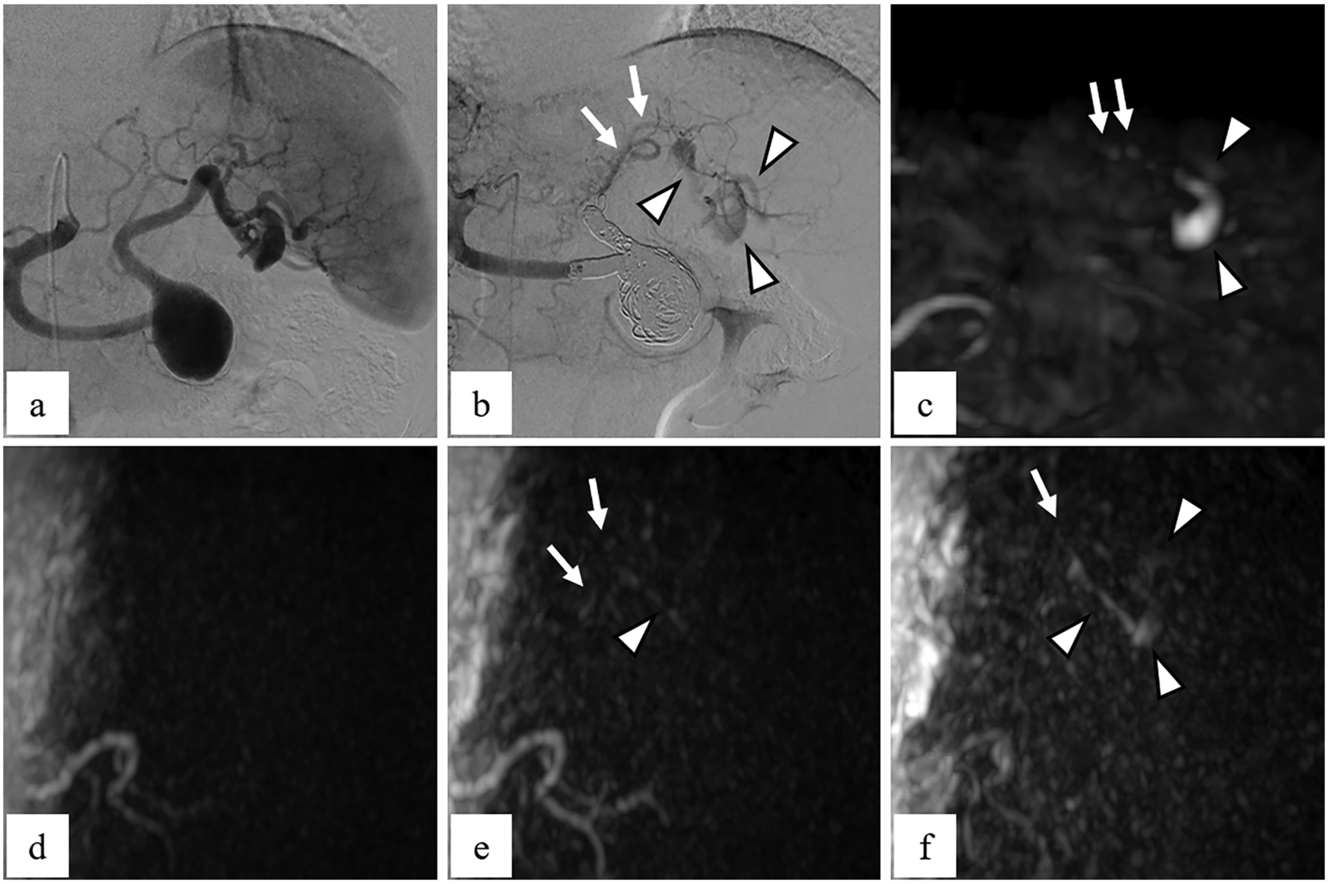

Fig. 4 A 71-year-old woman with a splenic artery aneurysm (Case 4). (**a**) Pre-treatment DSA of the celiac artery. (**b**) DSA after coil embolization by parent artery occlusion (isolation technique) combined with roughly aneurysmal coil packing showing complete embolization of the aneurysm and occlusion of the parent artery. The distal part of the parent artery (arrowheads) is preserved via the collateral arteries (arrows). (**c**) Follow-up TR-CEMRA performed three months after coil embolization (partial MIP image). No contrast effect is detected in the aneurysm, indicating complete occlusion. The distal part of the parent artery is visualized (arrowheads), and the collateral arteries are faintly delineated (arrows). (**d**–**f**) UTE-mASTAR MRA (partial MIP image). The delay times of images (**e**), (**f**), and (**g**) were 200, 506, and 812 ms, respectively. No evidence of aneurysmal recanalization as well as TR-CEMRA. The distal part of the parent artery (arrowheads) is gradually visualized via the collateral arteries (arrows). Note that UTE-mASTAR MRA more clearly depicts hemodynamics of the distal artery via collateral arteries. DSA, digital subtraction angiography; MIP, maximum intensity projection; TR-CEMRA, time-resolved contrast-enhanced MRA; UTE-mASTAR MRA, ultra-short TE MR angiography combined with modified signal targeting alternating radio frequency with asymmetric inversion slabs.

with metallic devices such as coils, vascular plugs, and stents.[20–24] Several clinical studies reported that UTE with or without the ASL technique reduces the susceptibility artifacts due to the metallic coils and stents in intracranial lesions.[21–24] However, applying this technique for the evaluation of vascular lesions in VAAs remains challenging because additional techniques, including respiratory and/or electrocardiogram synchronization, are required to acquire images of the body trunk. Recently, Mori et al. reported the application of UTE MRA with a time-spatial labeling inversion pulse, which is an ASL technique, for the assessment of a renal artery aneurysm treated with metallic coils.[12] This method enabled the visualization of the blood flow signals adjacent to the placed metallic coils, similar to our findings. However, their method could not provide serial hemodynamic images. To evaluate VAAs after coil embolization, it is important to assess the recanalization of the aneurysm and the patency of the parent artery and distal artery to the embolization site. Therefore, UTE-mASTAR MRA may be more suitable for the post-treatment evaluation of embolized VAAs. Furthermore, we confirmed the feasibility of UTE-mASTAR MRA for post-embolization evaluation of the renal artery and splenic and hepatic artery aneurysms, which suggests the wide applicability of this technique. Consistent with our findings, Hamamoto et al. reported the utility of UTE-mASTAR MRA in detecting recanalized pulmonary arteriovenous malformations after coil embolization.[25]

The fact that UTE-mASTAR MRA can provide high temporal resolution hemodynamic images with approximately 300 ms intervals is notable for post-embolization

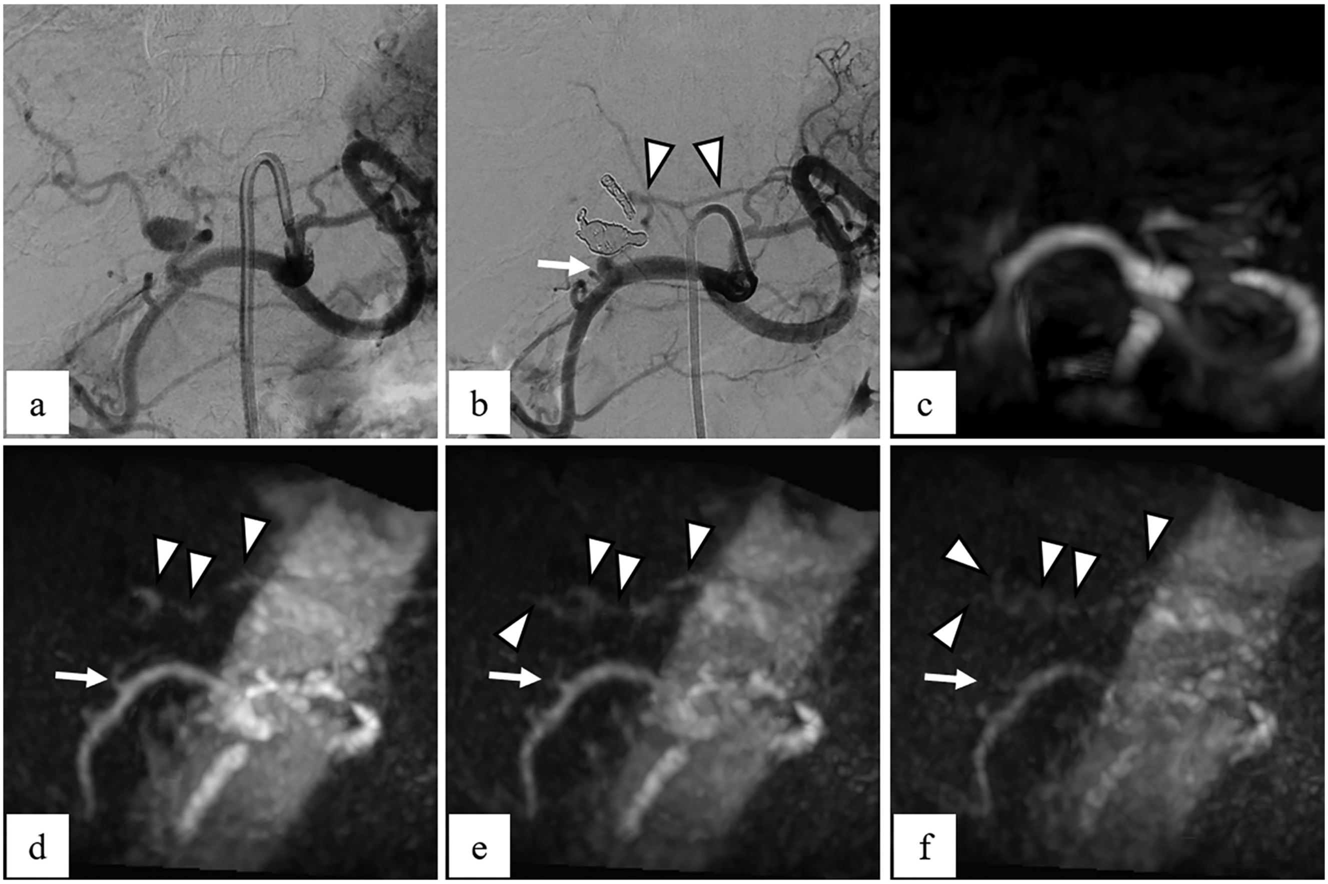

Fig. 5 A 71-year-old woman with a proper hepatic artery aneurysm (Case 5). (**a**) Pre-treatment DSA of the celiac artery. The right and middle hepatic arteries branch from the aneurysm. (**b**) DSA after coil embolization by parent artery occlusion (isolation technique) combined with roughly aneurysmal coil packing showing complete embolization of the aneurysm and occlusion of the right and middle hepatic artery. The proximal portions of the proper hepatic artery (arrow) and left hepatic artery are preserved (arrowheads). (**c**) Follow-up TR-CEMRA performed two months after coil embolization (partial MIP image). No contrast effect is detected in the aneurysm, indicating complete occlusion. The peripheral branches of the hepatic artery are unclear. (**d**–**f**) UTE-mASTAR MRA (partial MIP image). The delay time of images (**d**), (**e**), and (**f**) was 200, 506, and 812 ms, respectively. No evidence of aneurysmal recanalization as well as TR-CEMRA. The proximal part of the proper hepatic artery (arrows) and left hepatic artery (arrowheads) are clearly visualized, consistent with DSA after coil embolization. DSA, digital subtraction angiography; MIP, maximum intensity projection; TR-CEMRA, time-resolved contrast-enhanced MRA; UTE-mASTAR MRA, ultra-short TE MR angiography combined with modified signal targeting alternating radio frequency with asymmetric inversion slabs.

evaluation in VAAs. The acquisition of serial hemodynamic images with a high temporal resolution is essential to accurately determine the patency of the parent artery and recanalized aneurysms. Therefore, DSA is still used as a reliable method for assessment after coil embolization because it allows serial hemodynamic evaluation with fewer metallic artifacts.[1–3,5] Generally, the temporal resolutions of DSA and TR-CEMRA in the body trunk regions are approximately 200 ms and 2000–3000 ms, respectively.[10] Given that UTE-mASTAR MRA has a much higher temporal resolution than that of TR-CEMRA, which is comparable to DSA, this method is superior to TR-CEMRA in detecting the hemodynamic status of embolized lesions. Furthermore, UTE-mASTAR MRA directly delineated the continuity of the parent artery adjacent to the coils, which is difficult with TR-CEMRA. Taken together, UTE-mASTAR MRA can be an alternative to DSA or TR-CEMRA for the evaluation of VAAs after coil embolization.

UTE-mASTAR MRA has additional advantages over contrast-enhanced CT and MRA. First, this method does not require exposure to ionizing radiation or iodine- or gadolinium-based contrast agents, which may result in nephrotoxicity, anaphylaxis, nephrogenic systemic fibrosis, or tissue deposition of gadolinium. This characteristic may be particularly useful in patients with renal dysfunction or a history of adverse effects of contrast agents. Second, UTE-mASTAR MRA did not detect a thrombosis signal in the treated aneurysm because this method was reconstituted by subtracting the background image from the blood vessel image, which can reduce false-positives for assessing the

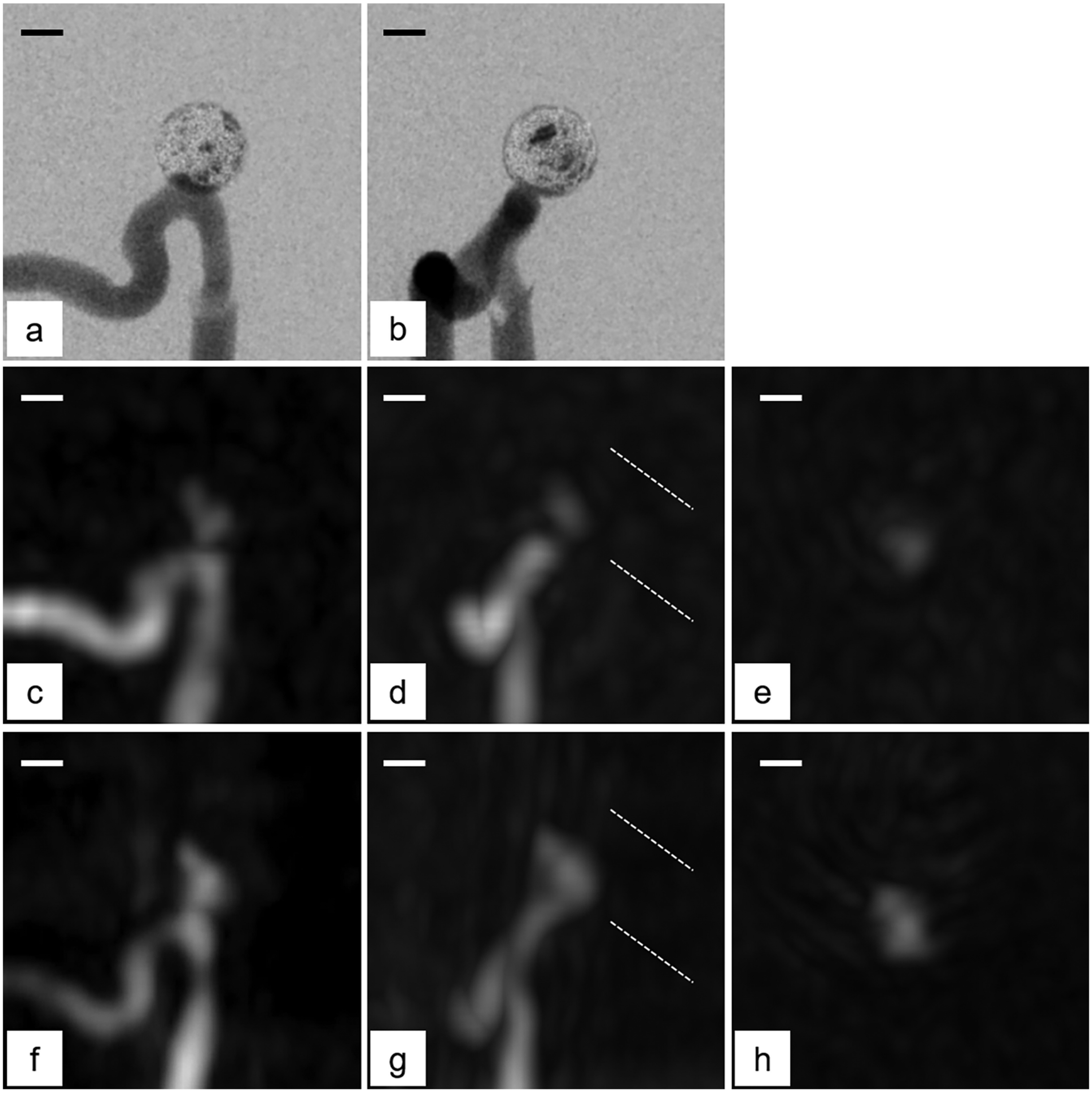

Fig. 6 Aneurysm phantom. (**a** and **b**) DSA of the coronal (0°) and sagittal (90°) view, respectively. Contrast effects are seen within the coil gap of the aneurysmal neck and body. (**c**–**e**) TR-CEMRA (partial MIP image). (**f**–**h**) UTE-mASTAR MRA with a delay time of 812 ms (partial MIP image). (**c** and **f**) Coronal view image corresponding to DSA. (**d** and **g**) Sagittal view image corresponding to DSA. (**e** and **h**) Oblique axial view image of the aneurysm phantom corresponding to the site indicated by the interval between the dashed lines in **d** and **g**. UTE-mASTAR MRA clearly depicts blood flow signals in both the neck and body of the aneurysm phantom compared to TR-CEMRA. The scale bar indicates 4 mm. DSA, digital subtraction angiography; MIP, maximum intensity projection; TR-CEMRA, time-resolved contrast-enhanced MRA; UTE-mASTAR MRA, ultra-short TE MR angiography combined with modified signal targeting alternating radio frequency with asymmetric inversion slabs.

intra-aneurysmal flow due to thrombi in the embolized aneurysm that may occur with contrast-enhanced MRA without the subtraction technique.[26] Third, UTE-mASTAR MRA has a relatively brief acquisition window in the late expiration phase, which is triggered by respiratory gating, resulting in a reduction-in-motion artifact, compared with TR-CEMRA which acquires images during breath-holding. Finally, the mUTE that we conducted in this study enables image acquisition with quite less acoustic noise than conventional UTE, which reduces the patient burden.

On the other hand, UTE-mASTAR MRA has some limitations compared to TR-CEMRA and CT. First, the acquisition time of the UTE-mASTAR MRA was approximately 10–13 min, which was much longer than that of

TR-CEMRA and CT. Second, the spatial resolution of UTE-mASTAR MRA is relatively low compared to that of CT or TR-CEMRA. Third, the SNR of UTE-mASTAR MRA tended to be lower than that of TR-CEMRA, particularly on images with longer delay time, although it did not affect the diagnostic performance. These drawbacks may be improved by using a higher magnetic-field MRI system which can enhance ASL capability and newly developed deep learning reconstruction methods to reduce image noise.[27] Finally, the capability of UTE-mASTAR MRA to detect minor signals from residual flow might depend on the packing density and embolic materials. However, the clinical implications of these minor residual blood flows are relatively low because they rarely require treatment.

The major limitations of the present study were the small sample size and lack of direct comparison between DSA and MRAs in the patient study. Regarding the latter, we did not perform follow-up DSA because it is an invasive procedure, and there were no cases of aneurysmal recanalization that required retreatment based on MRA findings. Although DSA is often used as the gold standard for evaluation after endovascular treatment, it is not always optimal because neck recanalization or coil compaction of aneurysms after embolization may be partially or totally masked by the radio-opaque coil mass. Additionally, the assessment of aneurysms after coil embolization using DSA is sometimes limited by the superimposition of arteries, particularly 2D assessment. Although validation studies are needed, the results of the phantom study would support the results of our patient study due to the high capability of UTE-mASTER MRA in detecting blood flow signals adjacent to the placed coils, comparable to DSA.

Conclusion

UTE-mASTAR MRA can provide high temporal resolution hemodynamic vascular images with fewer susceptibility artifacts without the use of a contrast agent. Our findings suggest that UTE-mASTAR MRA is a useful and feasible technique for the follow-up evaluation of VAAs after coil embolization.

Acknowledgments

We thank Yoshimasa Ikeda and Yusuke Ayabe for their technical advice regarding MRI.

Funding

This work was supported by JSPS KAKENHI (Grant Number JP18K15600).

Conflicts of Interest

The authors declare that they have no conflicts of interest.

References

1. Etezadi V, Gandhi RT, Benenati JF, et al. Endovascular treatment of visceral and renal artery aneurysms. J Vasc Interv Radiol 2011; 22:1246–1253.
2. Koganemaru M, Abe T, Nonoshita M, et al. Follow-up of true visceral artery aneurysm after coil embolization by three-dimensional contrast-enhanced MR angiography. Diagn Interv Radiol 2014; 20:129–135.
3. Laganà D, Carrafiello G, Mangini M, et al. Multimodal approach to endovascular treatment of visceral artery aneurysms and pseudoaneurysms. Eur J Radiol 2006; 59:104–111.
4. Tulsyan N, Kashyap VS, Greenberg RK, et al. The endovascular management of visceral artery aneurysms and pseudoaneurysms. J Vasc Surg 2007; 45:276–283;discussion 283.
5. Yasumoto T, Osuga K, Yamamoto H, et al. Long-term outcomes of coil packing for visceral aneurysms: correlation between packing density and incidence of coil compaction or recanalization. J Vasc Interv Radiol 2013; 24:1798–1807.
6. Hagspiel KD, Flors L, Hanley M, Norton PT. Computed tomography angiography and magnetic resonance angiography imaging of the mesenteric vasculature. Tech Vasc Interv Radiol 2015; 18:2–13.
7. Ikeda O, Tamura Y, Nakasone Y, Iryou Y, Yamashita Y. Nonoperative management of unruptured visceral artery aneurysms: treatment by transcatheter coil embolization. J Vasc Surg 2008; 47:1212–1219.
8. Iryo Y, Ikushima I, Hirai T, Yonenaga K, Yamashita Y. Evaluation of contrast-enhanced MR angiography in the follow-up of visceral arterial aneurysms after coil embolization. Acta Radiol 2013; 54:493–497.
9. Liu Q, Lu JP, Wang F, et al. Visceral artery aneurysms: evaluation using 3D contrast-enhanced MR angiography. AJR Am J Roentgenol 2008; 191:826–833.
10. Kawai T, Shimohira M, Suzuki K, et al. Time-resolved magnetic resonance angiography as a follow-up method for visceral artery aneurysm treated with coil-embolisation. Pol J Radiol 2018; 83:e137–e142.
11. Maruno M, Kiyosue H, Tanoue S, Hongo N, Kashiwagi J, Mori H. Unenhanced magnetic resonance angiography with time-spatial labeling inversion pulse for evaluating visceral artery aneurysms after endosaccular packing with detachable coils: preliminary results. J Vasc Interv Radiol 2013; 24:289–293.
12. Mori R, Kassai Y, Masuda A, et al. Ultrashort echo time time-spatial labeling inversion pulse magnetic resonance angiography with denoising deep learning reconstruction for the assessment of abdominal visceral arteries. J Magn Reson Imaging 2021; 53:1926–1937.
13. Ferrero E, Ferri M, Viazzo A, et al. Visceral artery aneurysms, an experience on 32 cases in a single center: treatment from surgery to multilayer stent. Ann Vasc Surg 2011; 25:923–935.
14. Takakura K, Kido A, Fujimoto K, et al. Evaluation of appropriate readout sequence for renal MRI perfusion using ASTAR (ASL) technique. Jpn J Radiol Technol 2016; 72:1105–1112. (in Japanese)
15. Watanabe K, Kurita K. Evaluation of three-dimensional contrast-enhanced MRA using differential rate k-space sampling (DRKS). Jpn J Radiol Technol 2002; 58:1609–1614. (in Japanese)

16. Stanisz GJ, Odrobina EE, Pun J, et al. T1, T2 relaxation and magnetization transfer in tissue at 3T. Magn Reson Med 2005; 54:507–512.
17. Kellman P, Chung YC, Simonetti OP, McVeigh ER, Arai AE. Multi-contrast delayed enhancement provides improved contrast between myocardial infarction and blood pool. J Magn Reson Imaging 2005; 22:605–613.
18. Sahbaee P, Segars WP, Marin D, Nelson RC, Samei E. The effect of contrast material on radiation dose at CT: part I. Incorporation of contrast material dynamics in anthropomorphic phantoms. Radiology 2017; 283:739–748.
19. Roy D, Milot G, Raymond J. Endovascular treatment of unruptured aneurysms. Stroke 2001; 32:1998–2004.
20. Ayabe Y, Hamamoto K, Ikeda Y, Koyama Y. Comparison of influence of susceptibility artifact due to metallic embolic material in MRA image. Jpn J Radiol Technol 2019; 75:460–467. (in Japanese)
21. Ayabe Y, Hamamoto K, Yoshino Y, et al. Ultra-short echo-time MR angiography combined with a subtraction method to assess intracranial aneurysms treated with a flow-diverter device. Magn Reson Med Sci 2021 December 11. [Epub ahead of print]
22. Irie R, Suzuki M, Yamamoto M, et al. Assessing blood flow in an intracranial stent: a feasibility study of MR angiography using a silent scan after stent-assisted coil embolization for anterior circulation aneurysms. AJNR Am J Neuroradiol 2015; 36:967–970.
23. Oishi H, Fujii T, Suzuki M, et al. Usefulness of silent MR angiography for intracranial aneurysms treated with a flow-diverter device. AJNR Am J Neuroradiol 2019; 40:808–814.
24. Takano N, Suzuki M, Irie R, et al. Non-contrast-enhanced silent scan MR angiography of intracranial anterior circulation aneurysms treated with a low-profile visualized intraluminal support device. AJNR Am J Neuroradiol 2017; 38:1610–1616.
25. Hamamoto K, Chiba E, Oyama-Manabe N, Shinmoto H. Ultra-short echo time magnetic resonance angiography using a modified signal targeting with alternative radio frequency spin labeling technique for detecting recanalized pulmonary arteriovenous malformation after coil embolization. Acta Radiol Open 2021; 10:20584601211057671.
26. Martin AJ, Hetts SW, Dillon WP, et al. MR imaging of partially thrombosed cerebral aneurysms: characteristics and evolution. AJNR Am J Neuroradiol 2011; 32:346–351.
27. Kidoh M, Shinoda K, Kitajima M, et al. Deep learning based noise reduction for brain MR imaging: tests on phantoms and healthy volunteers. Magn Reson Med Sci 2020; 19:195–206.